DOI 10.4430/bgo00370

Statistical analysis of the nowcasting approach for calculating assessments of the current state along the Iran-Iraq border

S.F. Mirhoseini[1], M. Mahood[2], N. Tahernia[3], A. Dorostian[1] and B. Akasheh[1]

[1] *Department of Geophysics, North Tehran Branch, Islamic Azad University, Tehran, Iran*
[2] *International Institute of Earthquake Engineering and Seismology (IIEES), Tehran, Iran*
[3] *Department of Physics, Parand Branch, Islamic Azad University, Parand, Iran*

(Received: 10 March 2021; accepted: 27 July 2021; published online: 18 January 2022)

ABSTRACT In this study, we examined concepts and applications deriving from the use of natural time to understand earthquake dynamics. In particular, the nowcasting concept is used to assess the current state of the fault system and its current level of progress through the earthquake cycle for Kermanshah city (as a centre of the Kermanshah province), in a radius circle of 500 km, as well as a seismic-prone region such as Sarpol-e Zahab and the surrounding area in radius circles of 100, 150, and 200 km. Of note, the nowcasting approach identifies a large seismically active geographic zone within which a local region of interest is embedded. Because statistical measurement of observed seismicity is critical for understanding earthquake dynamics and future risk, we computed the earthquake potential score (*EPS*) as the cumulative number of small earthquakes since the last large event in the studied region. The *EPS* values for occurrences with $M \geq 6.0$ within radius circles of 100, 150, and 200 km surrounding Sarpol-e Zahab city are 87, 93, and 96%, respectively.

Key words: nowcasting, Sarpol-e-Zahab, G-R law, completeness magnitude, earthquake potential score (*EPS*).

1. Introduction

This paper explores the concept of 'nowcasting', an idea arising from finance and economics (Rundle *et al.,* 2016), to evaluate the current status of the local earthquake fault system or development over the duration of frequent regional earthquakes. This is in contrast with the prediction, namely an estimation of the likelihood of potential significant earthquakes. The first use of natural time was used by Varotsos *et al*. (2005, 2011), and, then, by Holliday *et al.* (2006) with an emphasis on the application of the nowcasting method. It was also proposed that natural time analysis could be used in various areas. Recent studies have shown that nowcasting is a new technique for calculating the seismic risk level based on natural time (Rundle *et al.,* 2016, 2018, 2019, 2020; Luginbuhl *et al.,* 2018a, 2018b; Flores-Márquez *et al.,* 2020). We emphasise that the term 'earthquake cycle' applies to the frequent events in a seismically active region, but not to individual fault events (Sornette and Knopoff, 1997).

The nowcast method used here is not a model in that there are no free parameters to be fit to data. Rather, the method is simply a presentation of statistical data, which the user, then, interprets. The objective is to determine the amount of 'progress' of a seismically active region

through its earthquake cycle, which refers not to events on an individual fault, but to the recurring events in a seismically active region (Sornette and Knopoff, 1997).

Nowcasting, that describes the present state of a system, differs from forecasting, which looks forward in time (Holliday *et al.,* 2005, 2016; Field, 2007; Rundle *et al.,* 2012). Forecasting is the computation of future probability, whereas nowcasting is the assessment of the system's current state. If a method is employed to project the current state into future states, nowcasting can be utilised as a basis for forecasting. Actually, nowcasting should be considered a requirement for forecasting, or estimating the system's future state (Rundle *et al.,* 2016).

Earthquake nowcasting focuses on the assumption that powered threshold mechanisms, for instance earthquake fault systems, often present a power-law statistical distribution of magnitude consisting of small and large earthquake distributions. For earthquakes with an $M >$ 6.0, the greatest damage and number of injuries are incurred. Many small events with different sizes and magnitudes are interspersed between these large events (Pasari, 2019).

In this study, we consider the nowcasting approach to estimate the current level of earthquake hazard in the seismic-prone Kermanshah province and adjacent regions. We compute the earthquake potential score (*EPS*) for the seismically Sarpol-e Zahab region. We assume that the underlying seismicity statistics of locally defined circular regions are embedded in the Kermanshah province. This assumption seems reasonable in light of ergodic dynamics in the statistical physics of seismicity, in which the statistics of smaller regions over longer times are considered to be similar to the statistics of broader regions over large spatial domains and longer periods (Holliday *et al.,* 2016). In other words, we assume that the ensemble spatial average statistics of natural time would not be different from the time average resulting from mutually exclusive smaller seismotectonic subdomains (Tiampo *et al.,* 2003). The nowcasting method is implemented for large $M \geq 6.0$ events using natural time statistics of $4.4 \leq M < 6.0$ events that often cause damage to engineering structures and detrimental economic effects.

2. Basic nowcast method

The magnitude-frequency law of Gutenberg-Richter (G-R) (Gutenberg and Richter, 1942; Scholz, 1990) is a basic model that can be used to demonstrate that the number of small earthquakes with magnitudes greater than M_α but smaller than M_λ is the known value of N on average. It is noted that there are two parameters for the G-R model, namely a and b, which must be consistent with the data being observed:

$$\log_{10} N = a - bM \tag{1}$$

where the b-value denotes the ratio between the small and large events (which is nearly equal to 1 in seismically active regions), the a-value defines the background seismicity rate, and N is the number of earthquakes with a magnitude greater than M (Scholz, 1990). We consider small earthquakes of magnitude $4.4 \leq M < 6.0$, and large earthquakes of magnitude $M \geq 6.0$ that have occurred since 1 December 1955 and are derived from the U.S. Geological Survey (USGS), 2017 online catalogue. Considering the area identified in this study (Sarpol-e Zahab region) by a radius circle of 350 km, we use the natural time to calculate the current hazard of the defined seismically active area.

It would be rational to conclude that a large earthquake will occur in the fairly near future as seismicity continues to accumulate, given the general statement that 50 small earthquakes have occurred since the last large earthquake (Rundle *et al.,* 2020). Hence, the current risk level for earthquakes greater than $M > 6.0$ will be estimated to be high. Obviously, it could be years until the large earthquake might happen, but this is the universal concept behind this (Rundle *et al.,* 2020).

3. Results and discussion

3.1. Study area and earthquake data

In order to illustrate the nowcasting method in this work, we begin with nowcasts of the earthquake potential in the centre of Kermanshah province (Kermanshah city: lat. 34.31° N, lon. 47.07° E) with a radius of 500 km, as illustrated in Fig. 1. We obtain earthquake statistics as well as the present *EPS* values for earthquakes with magnitudes greater than $M_\lambda = 6.0$ in the entire region. We, then, turn to a region in radius circles of 100, 150, and 200 km around the Sarpol-e Zahab. We again obtain the present *EPS* values for earthquakes in this region greater than $M_\lambda = 6.0$. Since December 1955, there have been 21 earthquakes in the studied region (between latitudes 30° to 39° N and longitudes 42° to 53° E) with magnitudes $M_\lambda \geq 6.0$ (see Table 1). In this region, we use a completeness magnitude of $M_\alpha = 4.4$. It is worth noting that, according to the study by Rundle *et al.* (2016), we have enough data to span at least ~20 or larger earthquake cycles in the region. We, then, compute the *EPS*, which is defined as the cumulative probability distribution, $P[n < n(t)]$ for the current count $n(t)$ of the small earthquakes in the region.

As a simple example of using natural time method to rank the current hazard of a defined seismically active region, consider the region described by the radius circles up to 350 km surrounding the Sarpol-e Zahab region (lat. = 34.77°, lon. = 45.76°), and where the estimated value of b (as the slope) is nearly 1.19: there are approximately 64 earthquakes (M_α) $4.4 \leq M < 6.0$ (M_λ) for each $M \geq 6.0$ earthquake. Just prior to the M 6.3 earthquake in Sarpol-e Zahab on 25 November 2018, a total of 108 earthquakes with $4.4 \leq M < 6.0$ occurred at 21:48 local time (18:18 GMT) since 12 November 2017: a destructive earthquake ($M_w = 7.3$) happened 5 km north of Ezgeleh and 43 km north of Sarpol-e Zahab in the Kermanshah province of Iran, near the border of Iraq-Iran, causing hundreds of deaths and thousands of injuries and building damage and collapse, mostly in the Kermanshah (Maleki Asayesh *et al.,* 2018). Based on this, we can conclude the nowcast Sarpol-e Zahab ranking has returned to its preceding hazard level. The actual statistics of the observed number or frequency of earthquakes may deviate significantly from Eq. 1 over a smaller geographic area and shorter time periods.

As shown in Fig. 2, we are building the G-R number-magnitude statistics. Statistics defined by blue circle symbols are taken from all earthquakes with completeness magnitudes greater than 4.4 since 1955, while red square symbols are all earthquakes of magnitude $4.4 \leq M < 6.0$ from just after $M = 7.3$ from 12 November 2017 to 9 January 2020. The results have good fit at nearly all magnitude intervals with a G-R scaling line (red dash line) with a slope of ~1.19 (b ~1.19). The recording of similar data for all small earthquakes arising just after the maximum event (M 7.3, radius = 350 km) around the Sarpol-e Zahab is shown with the red square symbols. The blue dashed line is a G-R line with the alike deviation as the red dashed line for the vast area (b = 1.19). Furthermore, earthquake symbols in the large area closely follow the red dashed G-R line up to ~M 7.0 in the large region, while the blue dashed line below M 5.0 is closely followed by

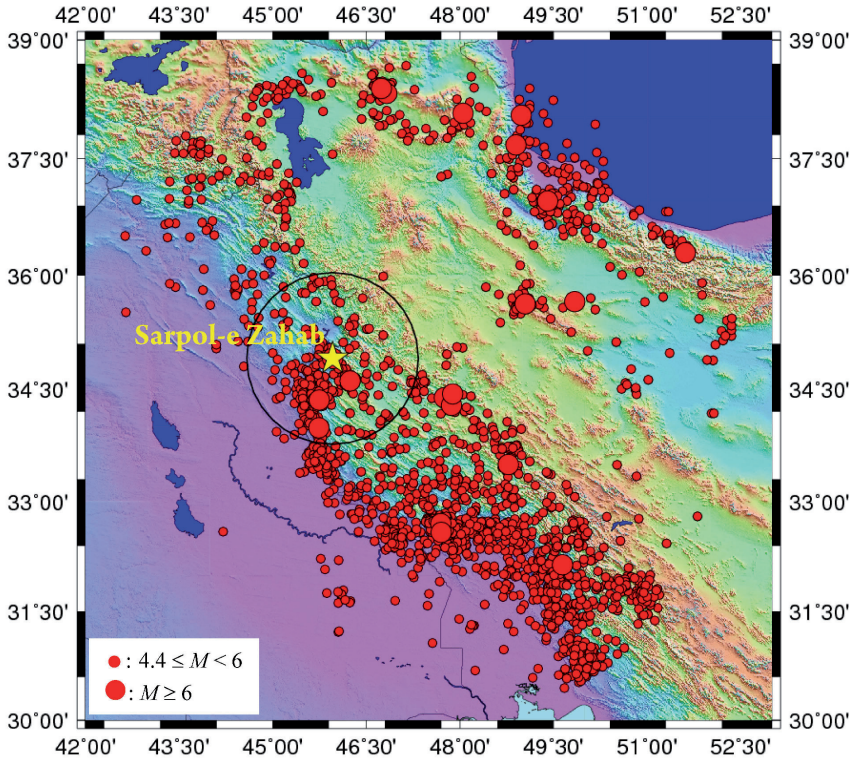

Fig. 1 - The region shown in this figure (Kermanshah province region) will be used to illustrate the nowcast method. We also consider the Sarpol-e Zahab region at the centre of the black circle with a radius of 200 km. Red dots represent events with $M_\lambda \geq 4.4$ for the period 1 December 1955 to 9 January 2020.

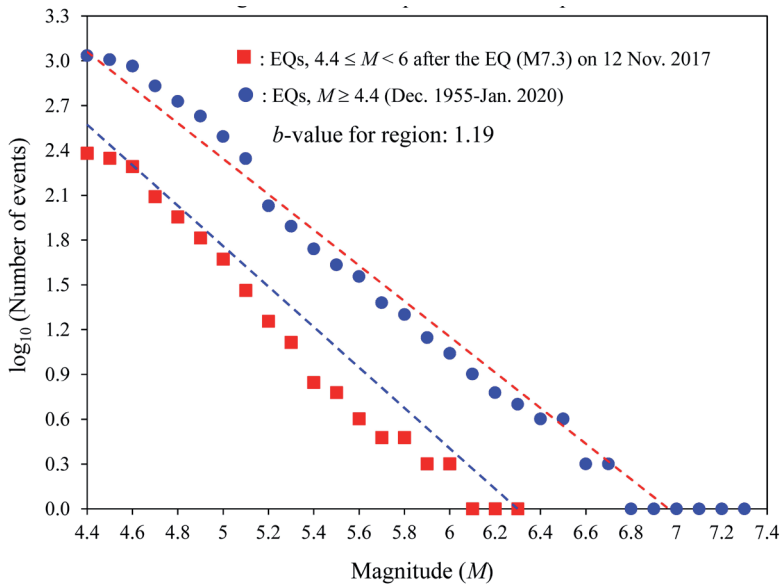

Fig. 2 - G-R magnitude frequency data of the Sarpol-e Zahab, Kermanshah-Iran (r = 350 km). The blue circles are all earthquakes with $M \geq 4.4$ for the studied area as a whole, from 1 December 1955 to 9 January 2020. The red squares are all earthquakes with $4.4 \leq M < 6.0$ after the last M 7.3 earthquake that occurred in the Sarpol-e Zahab region on 12 November 2017.

recent earthquakes (red square symbol). The red square symbols drop below the blue dashed line for earthquakes with $M > 5.0$. Thus, it seems there is a shortage of larger events that will finally be filled by the occurrence of large earthquakes, assuming that the G-R statistics are the same both in small and large areas.

Table 1 - List of earthquakes $M \geq 6.0$ occurring in the Kermanshah city in 1955 and later (r = 500 km).

No.	Date			Location		Magnitude (M_w)	Depth (km)	Interevent count of $4.4 \leq M_\alpha < 6.0$ events
	year	month	day	Lat. N (°)	Lon. E (°)			
1	1957	12	13	34.388	47.748	6.5	15	3
2	1958	8	16	34.29	47.867	6.7	15	3
3	1962	9	1	35.656	49.843	7.0	15	2
4	1963	3	24	34.438	47.882	6.0	20	2
5	1967	1	11	33.989	45.738	6.1	35	–
6	1977	4	6	31.983	50.683	6.0	41	71
7	1978	11	4	37.674	48.901	6.2	34	37
8	1978	12	14	32.139	49.646	6.2	33	–
9	1980	5	4	38.053	48.985	6.2	46	23
10	1990	6	20	36.957	49.409	7.4	18.5	272
11	1997	2	28	38.075	48.05	6.1	10	248
12	2002	6	22	35.626	49.047	6.5	10	170
13	2004	5	28	36.29	51.61	6.3	17	87
14	2006	3	31	33.5	48.78	6.1	7	114
15	2012	8	11	38.329	46.826	6.4	11	236
16	2012	8	11	38.389	46.745	6.2	12	1
17	2014	8	18	32.703	47.695	6.2	10.2	133
18	2014	8	18	32.5827	47.7037	6.0	5	36
19	2017	11	12	34.9109	45.9592	7.3	19	168
20	2018	8	25	34.6111	46.2422	6.0	10	173
21	2018	11	25	34.3609	45.7443	6.3	18	33

Since the greatest earthquake of magnitude M = 7.3 on 12 November 2017, the most powerful earthquake in this series was the M = 6.3 earthquake of 25 November 2018. It should be noted that the G-R relationship is not perfect in the sense that the data do not establish a linear scale relationship across the whole spectrum of magnitude. In particular, there is an obvious earthquake shortage greater than M 6.0, which will inevitably have to be filled at the high end if a linear G-R relationship is to be considered (see Fig. 2). Instead, the information in Fig. 2, after the earthquake of M = 6.3 on 25 November 2018, displays that the scaling line is re-established at the end of the small magnitude. The b-value of the scaling line in Fig. 3 is almost similar to that in Fig. 2, and there is a shortage in large earthquakes comparative to the scaling line. Finally, this shortage in large earthquakes is eliminated as large earthquakes occur.

The seismic moment relationship suggested by Hanks and Kanamori (1979) is a linear relationship of magnitude and the natural moment logarithm that would eventually be filled by the G-R distribution. It is, therefore, expected, on the basis of the principle of natural time, that this deficit will be gradually filled by the occurrence of large earthquakes over time.

The *M* 6.3 magnitude earthquake in the Sarpol-e Zahab region on 25 November 2018 is proof of this claim that can be justified by the least-squares method and we will reach an approximate number of ~6.3 along the blue dashed line and its intersection with the *X*-axis. Now, we wish to examine the same model for earthquakes with magnitude $M \geq 6.0$ after the 25 November 2018 earthquake; consequently, in the frequency diagram in Fig. 3, we examine the earthquakes after the *M* 6.3 earthquake. The red square symbols are clearly located below the blue line. According to the principle of natural time, the lack of earthquakes greater than 6.0 is explicitly known to be gradually filled by the occurrence of large earthquakes, and this shortage is expected to be filled over time. This would mean that an earthquake of *M* ~5.9 could be probable if the scales were to be preserved for all magnitudes (see Fig. 3).

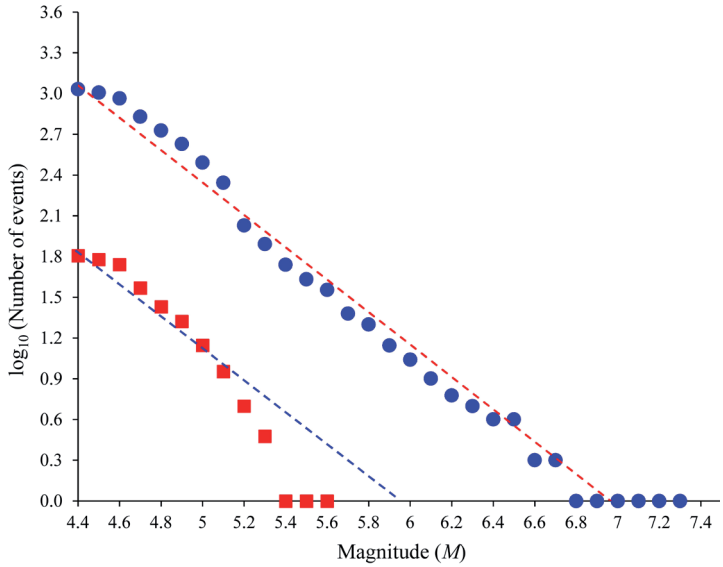

Fig. 3 - G-R number-magnitude statistics for the Sarpol-e Zahab region. The blue circles are all earthquakes with $M \geq 4.4$ for the area as a whole since 1955. The red squares are all earthquakes with $4.4 \leq M < 6.0$ after the last *M* 6.3 earthquake that occurred in the Sarpol-e Zahab region on 25 November 2018.

3.2. Average earthquake statistics

Driven threshold systems indicate some of the most self-organising systems, essentially non-linear in nature, including earthquake fault networks, the global web, and neural networks, as well as many social, ecological, and political systems (Fisher, 1985; Bak *et al.,* 1987; Gopal and Durian, 1995; Herz and Hopfield, 1995; Rundle *et al.,* 1995; Urbach *et al.,* 1995; Fisher *et al.,* 1997). These systems have dynamics that are closely associated with time and space having a multiplicity of temporal and spatial scales. If the correlations between the components are long and the coupling minimal, such that the dynamics can be viewed as a mean-field, the fluctuations tend to be suppressed and the system can reach a steady state (Tiampo *et al.,* 2003).

Because of the nature of the stress mechanism, the fundamental elastic behaviour between fault patches results in the creation of a mean-field regime for the earthquake system (Rundle *et al.,* 2018). In particular, a variety of studies revealed that simulations of statistically stationary, dissipative mean-field models effectively explain ergodic dynamics, and these model systems occur in a number of physical states that are close to or metastable (Thirumalai and Mountain, 1993; Rundle *et al.,* 1995; Ferguson *et al.,* 1999; Egolf, 2000).

The system evolves into an energy landscape approach related to the time-dependent system that occurs in one of the large number of scale-invariant free energy minima or wells that dotted the landscape (Wales, 2004). Fluctuations in the energy wells are attributed to the scale-invariant properties, power-law distributions, and the end of repetition of small earthquakes. As the topography of the landscape is regularly evolving, there will occasionally be times when the system escapes from its local energy well in a nucleation event, subsequently landing in another nearby energy well. The nucleation phenomenon is associated with a significant earthquake (Rundle *et al.,* 2018).

The ergodic property of the seismicity system is one in which the overall average gives the same result as the time average. The total average is likely to be the spatial average, in that a large seismically active region is considered to consist of non-overlapping subdomains of smaller seismic zones. Thirumalai and Mountain's (1993) metric was used to determine the ergodic properties of the seismicity systems. An ergodic system is one in which ensemble averages yield the same result as time averages (Rundle *et al.*, 2018). According to whatever is discussed by Rundle *et al.* (2018), the G-R scaling line was fitted over the magnitude interval 4.4–6.0 and yields a *b*-value of 1.19. As a result, by understanding the relationship, $b = [1.5 / (\tau - 1)]$, we implied that the value of $\tau = 2.26$ is close to the value of $\tau \sim 2.5$ characteristic of the mean-field and near to the main-field systems. Similarly, we find that the value for the mean-field systems is $\sigma = 0.89$. Klein *et al.* (2007), with relationship $\log_{10}[n(M)] = a - bM - 10^{1.5\,\sigma\,(M-M_0)}$, addressed the physical importance of this when applied to earthquakes.

The assumption that the values of scaling exponents (τ and σ), in particular their mean-field values, suggest that the seismicity is likely to have ergodic properties, and, therefore, the time averages should be equal to the overall or spatial averages (Rundle *et al.,* 2018). Instead, the shortage of large earthquakes in the G-R numbers means that eventually the occurrence of large earthquakes will have to be filled.

3.3. Nowcasting seismic risk

The key purpose is to characterise a number at a certain time for a specified small geographical area until the current potential for a large earthquake to happen in an area, which is vulnerable to repeated large earthquakes, is described (Rundle *et al.,* 2018). The earthquake cycle is described as the interval between two large earthquakes in a seismic area. We indicate the large earthquake magnitude as M_λ, which has the potential to cause reasonable damage if it occurs nearby it. We measure the potential by calculating small earthquakes, whose magnitude is indicated by M_α. The magnitude of the large earthquake is chosen to ensure that the appropriate earthquake interval will provide suitable statistics. The magnitude of small earthquakes is usually determined by the level of completeness of the catalogue, but can also be reported within a given range as a free parameter. The inter-event count of small earthquakes (magnitudes ranging from M_α to M_λ) for two successive large events is unpredictable (Rundle *et al.,* 2016). The aim of this work is to construct a cumulative distribution function (CDF) or probability density function (PDF) for small earthquake counts (Pasari, 2019). The CDF can be calculated by tabulating the number of small

earthquakes occurring between two large earthquakes and using standard methods (Bevington and Robinson, 2003).

It should be noted that one of the problems related to nowcasting is due to the fact that the catalogues of earthquakes are certainly not complete, especially for small magnitude earthquakes. Small events detected during the aftershock series may not be recorded in full due to instrumental problems. Another issue is that large earthquakes are of interest, which are undoubtedly limited in number compared to events that have several cycles of activity in the larger area. As a result of this constraint, the magnitude of large earthquakes is likely to be limited to approximately $M_\lambda \geq 6.0$. It is known that the basis for the nowcast is the utilisation of natural time, which is the calculation of small earthquakes after the last major earthquake. There are certain benefits of using natural time as follows:

1) there is no need to separate the aftershocks ('decluster') from the background seismicity;
2) specific statistics on natural events are used, instead of the amount of seismicity that is often acquired with respect to calendar time.

The G-R magnitude-frequency relationship (Scholz, 1990) may be used to show that the average number of small earthquakes with magnitude greater than M_α but less than magnitude M_λ is known as N. Using the G-R law, we can calculate N for an average number N_{avg} of earthquakes greater than M:

$$N_{\text{avg}} = 10^{a} \times 10^{-bM} \tag{2}$$

where the value of b is normally close to 1 and the value is determined by the level of seismicity in the area (Scholz, 1990). If we denote by $N_\alpha = 10^a \text{x} 10^{-bM\alpha}$ and $N_\lambda = 10^a \text{x} 10^{-bM\lambda}$, the average number of earthquakes with magnitudes greater than M_α and M_λ, respectively, thus we find (Rundle *et al.,* 2016):

$$N = \frac{N_\alpha - N_\lambda}{N_\lambda} = 10^{b(M_\lambda - M_\alpha)} - 1 \tag{3}$$

For the earthquake mechanism, the number of small earthquakes is also used as an indicator of the passing of natural time. Note that N is not dependent on a. The mean inter-event count will be named the average number N of small earthquakes among large earthquakes. Statistically, we can express the progress through the regional earthquake cicle, or potential for a large earthquake to occur with a magnitude greater than M_λ by calculating the CDF of small earthquakes with a magnitude greater than M_α but smaller than M_λ: $M_\alpha \leq M \leq M_\lambda$.

We organise the number of small earthquakes for every large earthquake period from the USGS earthquake catalogue to calculate the CDF. This is, then, used by standard methods to describe the PDF and the CDF (e.g. Bevington and Robinson, 2003). When we have acquired the CDF, the current number of small earthquakes $n(t)$ can, then, be used at time t to measure the current value of the CDF, $P[n \leq n(t)]$. Note that, after the last large earthquake, t is the (calendar) time, and $n(t)$ is the number of small earthquakes. This value is known as the *EPS* at the time t:

$$EPS = P[n < n(t)]. \tag{4}$$

In the distinct geographical area, the *EPS* value is known to be the potential of the next large earthquake with a magnitude greater than M_λ. Since the last large earthquake, *EPS* will rise monotonically over time. Right after the next large earthquake, it will return to *EPS* = 0, and, then, start to rise monotonically again before the next large earthquake happens. We note that the method of nowcasting, *a priori*, does not provide a model; it is merely a system of data tabulation and analysis. However, to the degree that the findings have significance, it is a clear way of estimating, via the seismic period of large earthquakes, the progress of an area. As our research is independent of the seismic activity scale, as seen in Eq. 3, it can be extended either to the large geographical area used for statistics or to some smaller area in the larger area.

3.4. Sensitivity analysis

The current work includes six candidate probability models from time-dependent and time-independent distributions, namely normal, lognormal, gamma, exponential, Weibull, and inverse Gaussian, to provide a comprehensive statistical analysis of earthquake interoccurrence times in the studied region. The Kolmogorov-Smirnov (K-S) test is recommended among goodness-of-fit tests for the comparison and validation of the considered distributions owing to two benefits, namely, its non-parametric nature and the ability to analyse the overall fitting analysis of the K-S plot (Johnson *et al.,* 1995). The cumulative distribution is the best fit model for evaluating the current number of small earthquake counts in the study region to provide a numerical *EPS* for the area (Mirhoseini *et al.,* 2021). The calculated K-S values for Kermanshah city with a radius of 500 km are listed in Table 2.

Table 2 - The estimated best fit distribution models using the K-S statistic test.

Distribution model	Normal	Lognormal	Gamma	Weibull	Exponential	Inverse Gaussian
K-S test	0.199868	0.204995	0.211280	0.198736	0.253777	0.715655

The *EPS* values for $M_\lambda \geq 5.5$ and 6.0 earthquakes in the region considered to be a circular zone were determined using small events of threshold magnitude M_α. We used the essential natural time statistics for the selected area to find the best-fit CDF. As can be seen in Table 3, the estimated K-S statistic values have shown that the Weibull distribution models are the best suited to reflect the present Sarpol-e Zahab earthquake catalogue and its surrounding areas under the considered conditions (M_α = 4.4; $M_\lambda \geq 5.5$ and 6.0). Furthermore, for a fixed threshold magnitude M_α, with a radius increasing from 100 to 200 km, the *EPS* value increased (Table 3).

Fig. 4 shows the results of the *EPS* value calculations for $M_\lambda \geq 5.5$ and 6.0 within 100-, 150-, and 200-km radius of the Sarpol-e Zahab area. The CDFs $P[n \leq n(t)]$ of the histogram values are shown by the blue curves. The number of small earthquakes since the last large earthquake is represented by the red circles. The thermometer on the right side is a visual depiction of the current cumulative probability, which specifies the *EPS* values for various radii and magnitudes M_λ. The red data-derived curve is the best fitting Weibull (1951) distribution. The obtained *EPS* score for $M \geq 5.5$ recovered to an average value of 72.3%, showing that this area is in a

comparatively mature seismic state, while the *EPS* findings for $M \geq 6.0$ are estimated to be 92%. By this measure, the Sarpol-e Zahab region is near the end of its current earthquake cycle for events $M \geq 6.0$ (see Table 3 and Fig. 4).

Table 3 - Earthquake potential scores around Sarpol-e Zahab and surrounding areas.

Parameters			*EPS* (%) score on 9 Jan. 2020	Natural time count on 9 Jan. 2020	Data last large event	Magnitude last large event	Best-fit model (K-S)
M_a	M_l	*r* (km)					
4.4	5.5	100	60	25	2019.01.06	5.6	Weibull
		150	75	33	2019.01.06	5.6	Weibull
		200	82	38	2019.01.06	5.6	Weibull
4.4	6.0	100	87	43	2018.11.25	6.3	Weibull
		150	93	51	2018.11.25	6.3	Weibull
		200	96	56	2018.11.25	6.3	Weibull

We used the natural time concept and the nowcasting approach to evaluate large earthquakes that occurred during the time period and in the study area to provide a seismic map of the considered geographical region. Fig. 5 depicts (Wessel and Smith, 1995) the estimated current *EPS* values as a risk map.

The increasing blue curve is the CDF = $P[n \leq n(t)]$ calculated from the large earthquake intervals. 64 earthquakes have occurred in the area with $M \geq 4.4$, since the last $M \geq 6.0$ on 25 November 2018, while for the last $M \geq 5.5$ on 6 January 2019, we had only 45 earthquakes. After the last large earthquake, the natural time count of $M \geq 6.0$ events using the cumulative number of small earthquakes *N* and the estimated current potential magnitude M_P of the forthcoming great earthquake at the present time is given by:

$$M_P = M_c + \left(\frac{1}{b}\right)\log_{10} N_s \tag{5}$$

where M_c reflects the catalogue completeness magnitude, N_s is the current count of small earthquakes increasing in time, and *b* denotes the G-R *b*-value. By applying Eq. 5 with $M_c = 4.4$, $b = 1.19$, and $N_s = 64$ in the Sarpol-e Zahab region, an approximation of the possible magnitude of the latest potential great earthquake as $M_P = 5.9$ can be found. This is consistent with the

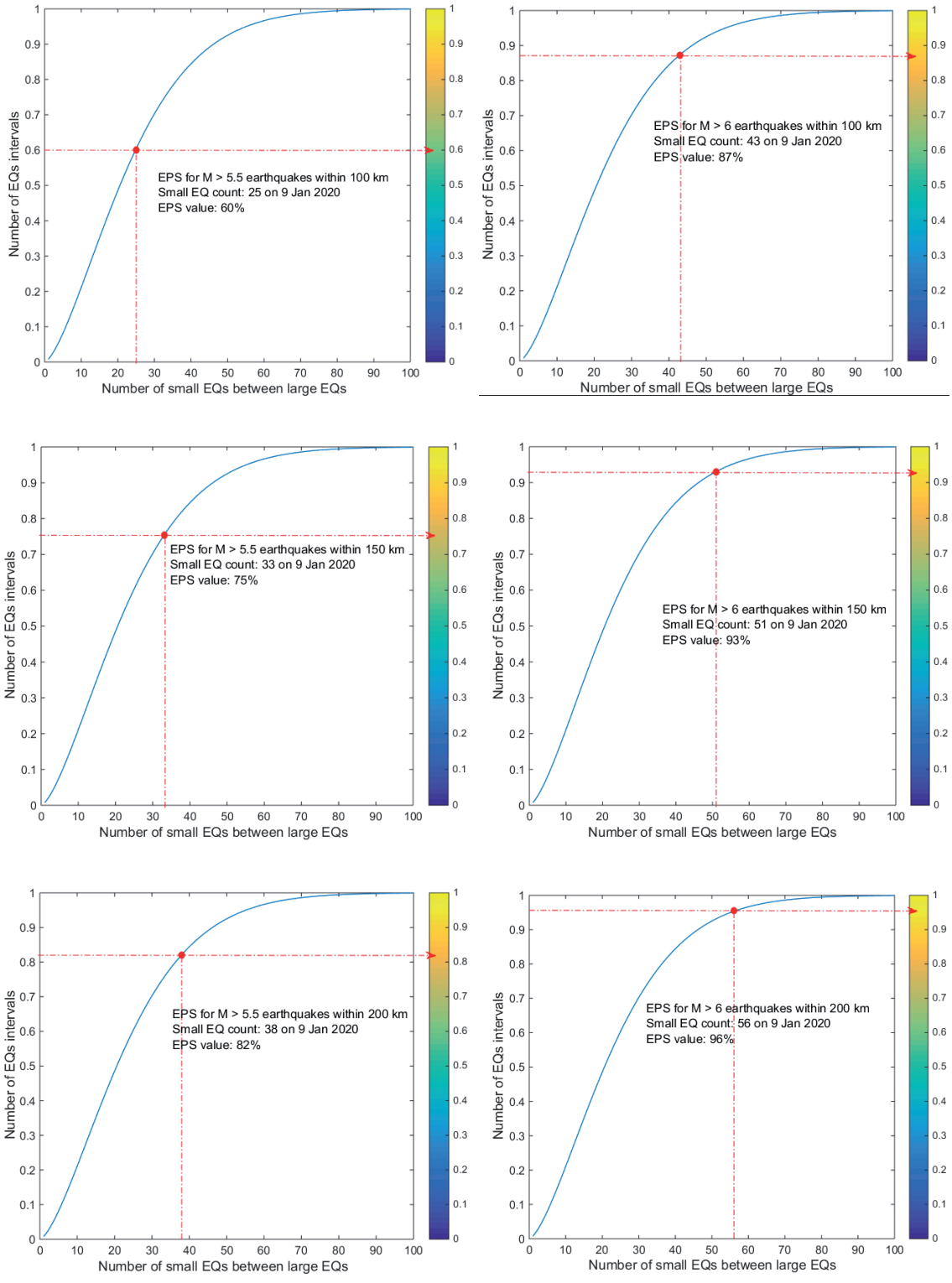

Fig. 4 - Nowcast for the $M \geq 5.5$ and 6.0 earthquakes in the Sarpol-e Zahab region. Blue curves are the best CDF. The red dots represent the current number of small earthquakes after the last large earthquake of M 5.5 and 6.0 on 6 January 2019 and 25 November 2018, respectively.

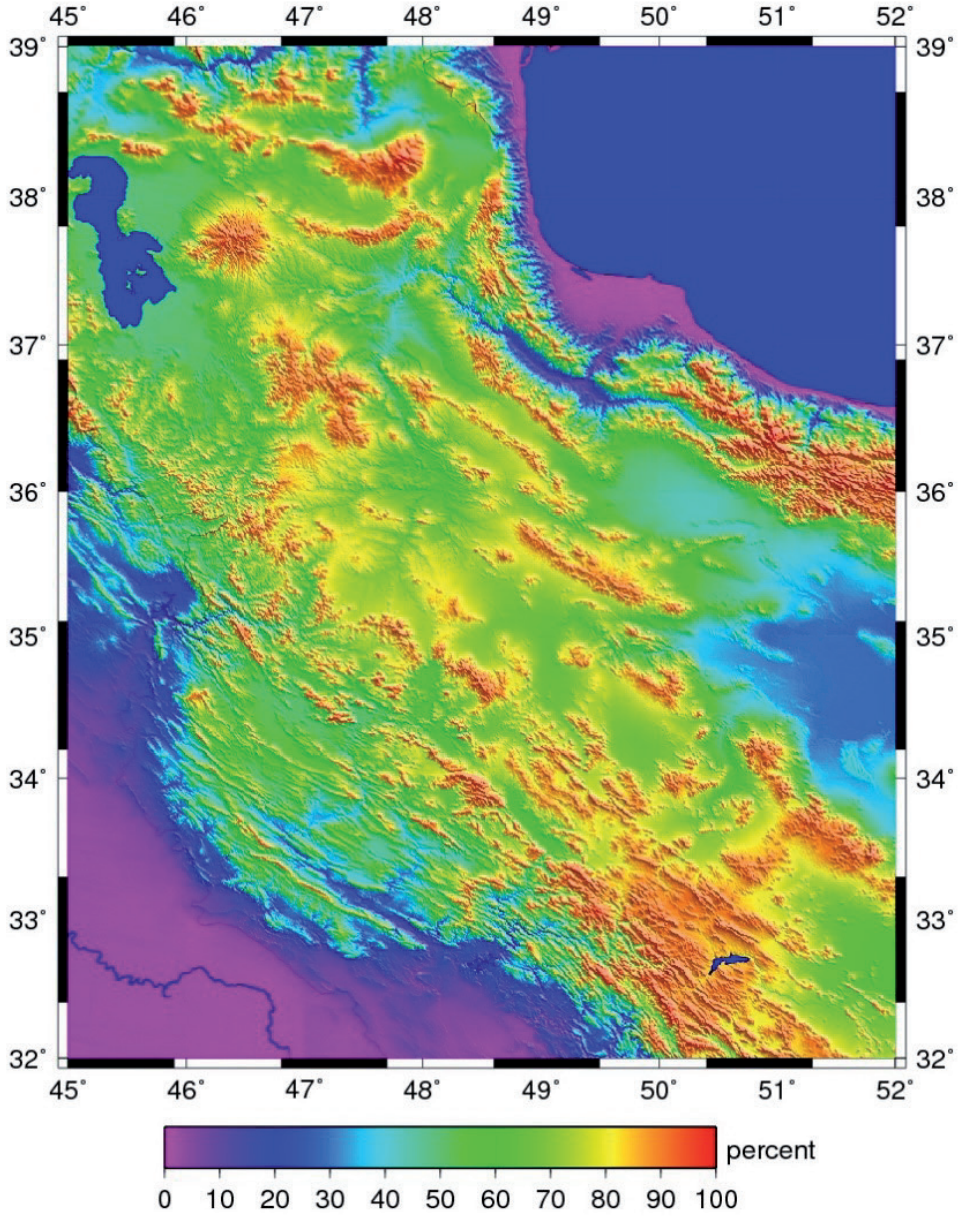

Fig. 5 - Current state of earthquake hazard for Kermanshah city with a radius of 500 km.

potential for the next earthquake in Fig. 2, which suggests that an earthquake with a magnitude of nearly 5.9 will occur in the near future. The current *EPS* for $M \geq 6.0$ is estimated at 50%, suggesting that the studied region is obviously halfway through its great earthquake cycle. The information we have downloaded from the global earthquake catalogue of the USGS is given "as it is", but results from different catalogues cannot be compared (Rundle *et al.,* 2020). However, the estimated threshold of completeness and the cut-off date, the date on which the catalogue is meant to be finished at the $M > 6.0$ rates, may differ.

Because the data was downloaded from the USGS global earthquake catalogue, we are unable to compare results from different catalogues. However, we can change the assumed completeness threshold, as well as the cut-off date, the date after which the catalogue is supposed to be complete at the $M \geq 4.4$ level. Because of the latest great earthquake of 12 November 2017, we have two different cut-off dates of 1 January 2013 and 1 January 2018 in order to calculate the *EPS* analysis for completeness magnitudes from $M_c = 4.2$ to 4.6 as seen in Table 4. In this regard, we have downloaded the data from 1 December 1955 to 9 January 2020 from the USGS global catalogue, with the indicated completeness magnitude to produce this table. We, then, used actual counts of small earthquakes after the indicated cut-off date. Prior to the cut-off date, small earthquake numbers were calculated on the basis of the small earthquake happening rate after the cut-off date and, then, calculated by the time span from the date of the large earthquake to the cut-off date. In order to obtain the average value of the *EPS* along with its expected error, we, then, measure the *EPS*'s sensitivity to changes in these parameters.

We determined a cut-off date for the Kermanshah region of 1 January 2013. As can be seen in Table 4, the *EPS* value is consistent with all the magnitudes of completeness studied and has the highest *EPS* value at 94%, using a completeness magnitude of $M_c = 4.4$. For this reason, as noted above, the two large earthquakes in the catalogue (see Table 1) for that region with *M* 6.4 and 6.2 occurred on 11 August 2012, and its high *EPS* value may be due to the occurrence of aftershocks later that led to a higher small earthquake count. On the other hand, this region has two larger earthquakes with $M \geq 6.0$ on 18 August 2014, which may have increased the number of foreshocks before the occurrence of the main shock. In addition, the *EPS* value increased up to 99% if the cut-off date is changed to 1 January 2018 (see Table 4). The explanation for this increase in *EPS* value is because the studied region had three significant earthquakes over the five-year period (from 1 January 2013 to 1 January 2018), two events on 18 August 2014 and one on 12 November 2017. It should be mentioned that another rationale for using 1 January 2018 as a cut-off date in this study is that we experienced two significant earthquakes with $M \geq 6.0$ on 25 August 2018 and 25 November 2018. Table 4 shows that changing M_c introduces just a few percent of uncertainty. However, the results reveal that changing the cut-off date from 2013 to 2018 has a significant impact if the major earthquake date shifts from before to after the cut-off date (see Table 4).

Table 4 - Sensitivity analysis and the earthquake potential scores (%) in a radius of 500 km around the Kermanshah city.

Cut-off date	Completeness magnitude					Average *EPS* (%)
	4.2	4.3	4.4	4.5	4.6	
2013/01/01	94	94	94	88	79	89.8
2018/01/01	99	99	99	98	97	98.4

4. Conclusion

In this study, we examined the natural time concept and applied it to the topic of assessing the current seismic state of a defined geographic area during a local earthquake. For dates between 1 December 1955 and 9 January 2020, we used the nowcasting approach to estimate earthquake hazards in Kermanshah province, namely Sarpol-e Zahab and the surrounding area. The nowcasting applicability requires that the studied seismicity satisfies the G-R frequency magnitude with a reasonable approximation. The least-squares fit of the truncated G-R gives $M_{max} \approx 7.0$.

Based on the previous studies involving the nowcasting approach, we defined a local region (Sarpol-e Zahab) in which one or more large earthquakes have occurred and that is an area of interest for analysing the local level of current hazard. We note that the selection of the local region is arbitrary. The basic assumption is that the statistics of the large region (Kermanshah city with a radius of 500 km) also characterise the statistics of the local region in terms of small earthquake occurrence. It should be emphasised that the nowcasting approach identifies a large seismically active geographic zone within which a local region of interest is embedded.

In the nowcasting approach, we calculate the CDF for the number of small earthquakes between large earthquakes during a sequence of earthquake cycles. The Weibull distribution proves to have the best goodness-fit tests within a radius of 500 km around the studied region. We calculated the *EPS* as the cumulative number of small earthquakes since the last large event because statistical measurement of observed seismicity is crucial for understanding earthquake dynamics and future risk. The *EPS* values for $M \geq 6.0$ occurrences within radius circles of 100, 150, and 200 km neighbouring Sarpol-e Zahab city are 87, 93, and 96%, respectively.

We also linked the outcome of a preceding study (Rundle *et al.,* 2018), that reported performance ergodic dynamics in seismicity areas, and the ensemble (spatial) averages should be interchangeable with temporal averages. This means that the long-term seismicity estimates of local areas may be comparable to the statistics on the seismicity of larger regions in a much shorter time span. We obtained $\tau = 2.26$ and $\sigma = 0.89$, which are close to the value of $\tau \sim 2.5$ and $\sigma = 1.0$. These characteristics of the mean-field systems explained the physical importance of this when applied to earthquakes. For significant earthquakes, namely $M \geq 6.0$, that happened after 2013, including two large earthquakes on 18 August 2014 (M = 6.2 and 6.0), the major earthquakes on 12 November 2017 (M = 7.3), 25 August 2018 (M = 6.0), and 25 November 2018 (M = 6.3), the method is fairly reliable in that it is relatively insensitive to the choice of the completeness magnitude (Table 4). The approach also relies on the hypothesis of completeness of the catalogue of earthquakes analysed after a given cut-off date.

Acknowledgments. We would like to acknowledge two anonymous reviewers who helped us to considerably improve our paper.

REFERENCES

Bak P., Tang C. and Weisenfield K.; 1987: *Self-organized criticality: an explanation of the 1/f noise*. Phys. Rev. Lett., 59, 381-384, doi: 10.1103/PhysRevLett.59.381.

Bevington P.R. and Robinson D.K.; 2003: *Data reduction and error analysis in the physical sciences*. McGraw-Hill, Boston, MA, USA, 336 pp.

Egolf D.A.; 2000: *Equilibrium regained: from nonequilibrium chaos to statistical mechanics.* Sci*.,* 287, 101-104, doi: 10.1126/science.287.5450.101.

Ferguson C.D., Klein W. and Rundle J.B.; 1999: *Spinodals, scaling, and ergodicity in a threshold model with long-range stress transfer*. Phys. Rev. E, 60, 1359-1373, doi: 10.1103/PhysRevE.60.1359.

Field E.H.; 2007: *Overview of the working group for the development of regional earthquake likelihood models (RELM).* Seismol. Res. Lett., 78, 7-16, doi: 10.1785/gssrl.78.1.7.

Fisher D.S.; 1985: *Random fields, random anisotropies, nonlinear σ models, and dimensional reduction*. Phys. Rev. B, 31, 7233-7251, doi: 10.1103/PhysRevB.31.7233.

Fisher D.S., Dahmen K., Ramanathan S. and Ben-Zion Y.; 1997: *Statistics of earthquakes in simple models of heterogeneous faults*. Phys. Rev. Lett., 78, 4885-4888, doi: 10.1103/PhysRevLett.78.4885.

Flores-Márquez E.L., Ramírez-Rojas A., Perez-Oregon J., Sarlis N.V., Skordas E.S. and Varotsos P.A.; 2020: *Natural time analysis of seismicity within the Mexican flat slab before the M 7.1 earthquake on 19 September 2017*. Entropy, 22, 730, doi: 10.3390/e22070730.

Gopal A.D. and Durian D.J.; 1995: *Nonlinear bubble dynamics in a slowly driven foam*. Phys. Rev. Lett., 75, 2610-2613, doi: 10.1103/PhysRevLett.75.2610.

Gutenberg B. and Richter C.F.; 1942: *Earthquake magnitude, energy, intensity and acceleration*. Bull. Seismol. Soc. Am., 32, 163-191, doi: 10.1785/BSSA0320030163.

Hanks T.C. and Kanamori H.; 1979: *A moment magnitude scale.* J. Geophys. Res. Solid Earth, 84, 2348-2350, doi: 10.1029/JB084iB05p02348.

Herz A.V.M. and Hopfield J.J.; 1995: *Earthquake cycles and neural reverberations: collective oscillations in systems with pulse-coupled threshold elements*. Phys. Rev. Lett., 75, 1222-1225, doi: 10.1103/PhysRevLett.75.1222.

Holliday J.R., Nanjo K.Z., Tiampo K.F., Rundle J.B. and Turcotte D.L.; 2005: *Earthquake forecasting and its verification.* Nonlinear Processes Geophys., 12, 965-977, doi: 10.5194/npg-12-965-2005.

Holliday J.R., Rundle J.B., Turcotte D.L., Klein W., Tiampo K.F. and Donnellan A.; 2006: *Using earthquake intensities to forecast earthquake occurrence times*. Nonlinear Processes Geophys., 13, 585-593, doi: 10.5194/npg-13-585-2006.

Holliday J.R., Graves W.R., Rundle J.B. and Turcotte D.L.; 2016: *Computing earthquake probabilities on global scales.* Pure Appl. Geophys., 173, 739-748, doi: 10.1007/s00024-014-0951-3.

Johnson N.L., Kotz S. and Balakrishnan N.; 1995: *Continuous univariate distributions, 2nd ed.* Wiley-Interscience, New York, NY, USA, vol. 2, 752 pp.

Klein W., Gould H., Gulbahce N., Rundle J.B. and Tiampo K.F.; 2007: *Structure of fluctuations near mean-field critical points and spinodals and its implication for physical processes*. Physical Review E, 75(3), 031114, doi: 10.1103/PhysRevE.75.031114.

Luginbuhl M., Rundle J.B., Hawkins A. and Turcotte D.L.; 2018a: *Nowcasting earthquakes: a comparison of induced earthquakes in Oklahoma and at the Geysers, California*. Pure Appl. Geophys., 175, 49-65, doi: 10.1007/s00024-017-1678-8.

Luginbuhl M., Rundle J.B. and Turcotte D.L.; 2018b: *Natural time and nowcasting earthquakes: are large global earthquakes temporally clustered?* Pure Appl. Geophys., 175, 661-670, doi: 10.1007/ s00024-018-1778-0.

Maleki Asayesh B., Zafarani H. and Najafi N.; 2018: *Correlation between Coulomb stress change and aftershocks distribution in Sarpol-e-Zahab earthquake*. In: Proc. 18th Iranian Geophysical Conference, Tehran, Iran, pp. 1149-1152.

Mirhoseini S.F., Mahood M., Tahernia N., Dorostian A. and Akasheh B.; 2021: *Case study of earthquake probability using natural time and nowcasting of the Sarpol-e Zahab region in Kermanshah, Iran.* Pure Appl. Geophys., 178, 1181-1191, doi: 10.1007/s00024-021-02699-x.

Pasari S.; 2019: *Nowcasting earthquakes in the Bay of Bengal region*. Pure Appl. Geophys., 176, 1417-1432, doi: 10.1007/s00024-018-2037-0.

Rundle J.B., Klein W., Gross S. and Turcotte D.L.; 1995: *Boltzmann fluctuations in numerical simulations of nonequilibrium lattice threshold systems*. Phys. Rev. Lett., 75, 1658-1661, doi: 10.1103 /PhysRevLett.75.1658.

Rundle J.B., Holliday J.R., Graves W.R., Turcotte D.L., Tiampo K.F. and Klein W.; 2012: *Probabilities for large events in driven threshold systems.* Phys. Rev. E, 86, 021106.

Rundle J.B., Turcotte D.L., Donnellan A., Grant-Ludwig L., Luginbuhl M. and Gong G.; 2016: *Nowcasting earthquakes*. Earth Space Sci., 3, 480-486, doi: 10.1002/2016EA000185.

Rundle J.B., Luginbuhl M., Giguere A. and Turcotte D.L.; 2018: *Natural time, nowcasting and the physics of earthquakes: estimation of seismic risk to global megacities*. Pure Appl. Geophys., 175, 647-660, doi: 10.1007/s00024-017-1720-x.

Rundle J.B., Giguere A., Turcotte D.L., Crutchfield J.P. and Donnellan A.; 2019: *Global seismic nowcasting with Shannon information entropy*. Earth Space Sci., 6, 191-197, doi: 10.1029/2018EA00 0464.

Rundle J.B., Luginbuhl M., Khapikova P., Turcotte D.L., Donnellan A. and McKim G.; 2020: *Nowcasting great global earthquake and tsunami sources*. Pure Appl. Geophys., 177, 359-368, doi: 10.1007/s00024-018-2039-y.

Scholz C.H.; 1990: *The mechanics of earthquakes and faulting*. Cambridge University, Cambridge, UK, 451 pp., doi: 10.1126/science.250.4988.1758-a.

Sornette D. and Knopoff L.; 1997: *The paradox of the expected time until the next earthquake*. Bull. Seismol. Soc. Am., 87, 789-798.

Thirumalai D. and Mountain R.D.; 1993: *Activated dynamics, loss of ergodicity, and transport in supercooled liquids*. Phys. Rev. E, 47, 479-489, doi: 10.1103/PhysRevE.47.479.

Tiampo K.F., Rundle J.B., Klein W., Sá Martins J.S. and Ferguson C.D.; 2003: *Ergodic dynamics in a natural threshold system*. Phys. Rev. Lett., 91, 238501, doi: 10.1103/PhysRevLett.91.238501.

U.S. Geological Survey; 2017: *Earthquake facts and statistics*. Reston, VA, USA, Accessed 22 March 2018 at URL.

Urbach J.S., Madison R.C. and Markert J.T.; 1995: *Interface depinning, self-organized criticality, and the Barkhausen effect*. Phys. Rev. Lett., 75, 276-279, doi: 10.1103/PhysRevLett.75.276.

Varotsos P.A., Sarlis N.V., Tanaka H.K. and Skordas E.S.; 2005: *Some properties of the entropy in the natural time*. Phys. Rev. E, 71, 032102, doi: 10.1103/PhysRevE.71.032102.

Varotsos P.A., Sarlis N.V. and Skordas E.S.; 2011: *Natural time analysis: the new view of time*. Springer, Berlin, Germany, 476 pp., doi: 10.1007/978-3-642-16449-1.

Wales D.J.; 2004: *Energy landscapes: applications to clusters, biomolecules and glasses*. Cambridge University, Cambridge, UK, 692 pp., ISBN 978-0-511-72172-4.

Weibull W.; 1951: *A statistical distribution function of wide applicability.* J. Appl. Mech., 18, 293-297, doi: 10.1115/1.4010337.

Wessel P. and Smith W.H.F.; 1995: *New version of the Generic Mapping Tools released.* EOS Trans. Amer. Geophys. Union, 76, 329, doi: 10.1029/95EO00198.

Corresponding author: Majid Mahood
International Institute of Earthquake Engineering and Seismology (IIEES)
Arghavan St. 21, North Dibajee, Farmanieh, Tehran, Iran
Phone: +98 912 3854194; e-mail: m.mahood@iiees.ac.ir